3 Biotech (2016) 6:1
DOI 10.1007/s13205-015-0313-6

ORIGINAL ARTICLE

Unexpected formation of *N*′-phenyl-thiophosphorohydrazidic acid *O*,*S*-dimethyl ester from acephate: chemical, biotechnical and computational study

Vijay Kumar[1,4] · Sukhmanpreet Kaur[1] · Simranjeet Singh[2] · Niraj Upadhyay[3]

Received: 24 March 2015 / Accepted: 1 December 2015 / Published online: 23 December 2015

Abstract By the nucleophilic attack of phenylhydrazine on acephate in aqueous medium, a stable product *N*′-phenyl-thiophosphorohydrazidic acid *O*,*S*-dimethyl ester (**1**) was obtained and characterized by elemental, spectral and thermal analysis. Thermodynamic parameters, Ea, $\Delta H°$, $\Delta S°$ and $\Delta G°$, have found to be 62.15, −67.95, −0.068 and −20.05 kJ mol^{-1} according to the Coats–Redfern equation. Analysis of interaction of **1** with BSA protein was done by using the UV–Vis and FTIR spectroscopic methods. The observed binding constants was 1.12 (±0.09) × 10^4 M^{-1}. The biological effect of **1** was checked on different plant growth-promoting (PGPR) strains such as *Rhizobium leguminosarum*, *Pseudomonas fluorescens*, *Arthrobacter citreus*, *Bacillus brevis* and *Salmonella typhimurium* and compared with parent molecule acephate where **1** has shown less toxicity against PGPRs as compared to acephate. The experimental results for geometric parameters and values of peak position in IR spectra have found to match excellently with the computational studies performed by GAMESS software package. Theoretically, twelve new analogs of **1** were prepared and their comparative reactivity (HOMO–LUMO energy) and biodecomposition (on the basis of polarizability) is discussed.

Keywords Acephate · Phenylhydrazine · Thermal analysis · Plant growth-promoting traits

Introduction

All the contaminants including insecticides, nematodes and herbicides applied to crops reach to soil and influence the soil fertility by inhibiting the soil's microorganisms. Moreover, plant protection has become necessary in order to increase the food production, and therefore, multiple and over use of pesticides are called necessary evil (David 1998; Krämer 2007; Prasad et al. 2013; Wasim et al. 2009). Pesticides are considered to be an integral part of modern agriculture. So the topics such as green decomposition, production of less toxic and green pesticides are the prime most requirements of current era.

Acephate is an important and cheapest organophosphorus insecticide used worldwide (Kumar et al. 2015a). In last 5 years, every year 10 % increase in production of technical grade acephate was observed (Kumar et al. 2015a). It was registered to control a wide range of insects on various agricultural crops. The insecticidal potency of acephate is due to the inhibition of acetyl-cholinesterase (AChE) activity (Kumar et al. 2013a, 2015a). It is toxic in various components of the environment and further decomposed into highly toxic methamidophos (Kumar et al. 2015a). Hence, the safe decomposition and preparation of less toxic analog of acephate are an important issue from the environmental concern.

Electronic supplementary material The online version of this article (doi:10.1007/s13205-015-0313-6) contains supplementary material, which is available to authorized users.

✉ Niraj Upadhyay
nivij.res@gmail.com

[1] Department of Chemistry, Lovely Professional University, Punjab 144411, India

[2] Department of Biotechnology, Lovely Professional University, Punjab, India

[3] Department of Chemistry, Dr. Harisingh Gour University, Sagar, Madhya Pradesh, India

[4] Regional Pesticides Testing Laboratory, Ministry of Agriculture, Government of India, Chandigarh 160030, India

Moreover, phenylhydrazine is classified among the aromatic nucleophile. It acts as an intermediate of various active compounds (Chen et al. 2014; Rosamilia et al. 2008). As per our best information, there is no reported data about the interactions of phenylhydrazine with acephate. Accordingly, the present study (in vitro) was initiated to investigate the ability of phenylhydrazine to decompose/neutralize the toxic effect of acephate and synthesis of green pesticide.

Experimental

Materials

Acephate technical grade (>90 %) was supplied by Gautmi Ltd., Andhra Pradesh, India. All the materials and solvents employed in synthesis were of extra-pure grade and used after further purification. Pure cultures of the strains, namely *Rhizobium leguminosarum* (NCIM-2749), *Pseudomonas fluorescens* (NCIM-5096), *Arthrobacter citreus* (NCIM-2320), *Bacillus brevis* (NCIM-2532) and *Salmonella typhimurium* (NCIM-2501), were purchased from National Chemical Laboratory, Pune, India.

Chemistry

Decomposition/synthesis procedure

An environment-friendly one-step method was designed and followed where equimolar aqueous solution of acephate (0.018 g in 10 mL/0.01 M) mixed with one molar aqueous solution of phenylhydrazine (0.011 g in 10 mL/0.01 M) in a beaker. Solution of the beaker was stirred for 1 h at room temperature (RT) at pH 3 and kept for 7 days in the presence of normal light at RT and pH 3 (maintained by using HCl). Fine amorphous white-colored product (**1**) was obtained, which was washed with hot water, methanol and dried overnight at 45 °C and allowed for spectral, thermal, BSA binding and plant growth-promoting activities.

Biology

Plant growth-promoting activities

As mentioned above, entire pollutants including insecticides, nematodes and herbicides applied to crops reach to soil and influence soil fertility by inhibiting the soil's microorganisms. Hence, the study of the effect of newly synthesized molecule was seen on PGPR strains. In the current study, the plant growth-promoting activities, namely siderophore production, indole acetic acid production, hydrogen cyanide production and phosphate solubilization, were checked with above-mentioned strains (Kumar et al. 2015b). All the activities were preformed in triplicates, and results were analyzed by using the ANOVA statistical analysis.

*Preparation of stock solution and interaction of **1** with BSA*

Bovine serum albumin (40 mg/mL or 0.5 mM) was dissolved in aqueous solution containing phosphate buffer (pH 7.2). The protein concentration was determined spectrophotometrically using an extinction coefficient of 36,500 M^{-1} cm^{-1} at 275 nm (Painter et al. 1998). Solutions of **1** were first prepared in phosphate buffer/ethanol (50 %) and then diluted by serial dilution to 0.010, 0.0075, 0.0050, 0.0025, 0.00125 mM in the same phosphate buffer.

The absorption spectra were recorded on a Shimadzu 1800S double-beam spectrophotometer, using a slit of 5 nm; quartz cuvettes of 1 cm and scan speed of 250 nm min^{-1} were used. The UV–Vis absorptions of BSA in the presence and absence of **1** were measured at pH 7.2 by keeping the concentration of BSA constant (0.05 mM), while varying the concentration of **1** (0.010, 0.0075, 0.0050, 0.0025, 0.00125 mM), in the range of 230–400 nm. The binding constants of the drugs–BSA complexes were calculated as reported (mathematical detail is stated in Supplementary Information S3) (Abdi et al. 2012; Connors 1987).

FTIR spectroscopy measurements

Infrared measurement was taken at room temperature on a Shimadzu 8400S FTIR spectrometer, equipped with KBr beam splitter. FTIR study was performed as described by Abdi et al. (2012). Solution of **1** was added dropwise to the protein solution with constant stirring to ensure the formation of homogeneous solution. Interferograms were accumulated over the spectral range 4000–400 cm^{-1} with a nominal resolution of 4 cm^{-1} and 50 scans. At first, spectra of buffer (phosphate pH 7.4) and protein solution were collected on the same conditions. Then, buffer spectrum is subtracted from the spectra of sample solution to get the FTIR spectra of protein. The difference spectra [(protein solution + molecule solution) + (protein solution)] were generated using the polypeptide antisymmetric and symmetric C–H stretching bands located at 2900–2800 cm^{-1}, as internal standard. These bands, which are due to protein C–H stretching vibrations, do not undergo any spectral changes (shifting or intensity variation) upon any interaction with drug, and therefore, they are commonly used as internal standard. When producing difference spectra, these bands were adjusted to the baseline level, in order to normalize difference spectra.

Computational study

The theoretical, geometric parameters (bond lengths and bond angles, Huckel charge densities), polarizability, HOMO–LUMO energy difference and infrared intensities of the product in the ground state were calculated using HF method with the 6-311++G(d,p) basis set for the first time. Entire analysis was performed by GAMESS program package (Aihara 1999; Kumar et al. 2015c, d). The motive of the computational study was to assist and cross-check the experimental study and vice versa. Additional motive was to obtain the data such as steric energy, chemical reactivity, biodecomposition, Huckel charge densities, bond angles and bond length which are not experimentally obtained.

Results and discussions

Chemistry

Structure illustration

The observed values of absorption maxima (λ_{max}) for **1** in UV–Vis spectra were 269 nm (due to n → π* transitions) and 456 nm (due to π → π* transitions). By comparing the UV–Vis spectra of acephate with product (Fig. 1), it was observed that **1** contains an organic chromophoric group that leads to increase in wavelength as well as absorption. Comparatively, no sharp absorption maxima (λ_{max}) were observed in the case of acephate even in UV region. Here, UV–Vis spectra clearly indicate the formation of product due to bond formation of phenylhydrazine with acephate.

On comparison of IR spectra of acephate (IR spectra) and phenylhydrazine to **1**, new peak was observed at 3650 cm^{-1} that corresponds to stretching frequencies of free O–H of water. Broadening and shifting were observed in the stretching frequencies of N–H (3500–3300 cm^{-1}) of phenylhydrazine and acephate. A new peak at 2190 cm^{-1} was observed due to stretching vibration of C=N=N type allene system. Redshift in the stretching band of C=N group of **1** (1630 cm^{-1}) compared to phenylhydrazine (1900 cm^{-1}) was observed. The *v*(C=O) stretching band of acephate disappears in **1** that indicates removal of carbonyl group from acephate on attack of phenylhydrazine for the formation of **1**. Broad peak at 1500 cm^{-1} in **1** belongs to the stretching frequencies of C=C. Association of P=O oxygen with hydrogen atom of water molecule was observed in terms of broadening and increase in intensity of P–O stretching band (850 cm^{-1}) (Fig. 2). The frequency for N–H out of plane was observed at 700 cm^{-1} in broad and intense form (Kumar et al. 2013a, b; Silberstein et al. 2005).

Compound **1** displayed molecular ion peak at *m*/*z* 227.3 with relative abundance of 100 %, which is in excellent agreement with the structure shown in Fig. 3a. Hundred percentage intensity at 227.3 confirms the formation of a stable moiety *N*′-phenyl-thiophosphorohydrazidic acid *O*,*S*-dimethyl ester. Some other observed fragments with approximate intensity were at *m*/*z* = 159.4 (35 %) and 91.4 (40 %), respectively. In the fragmentation of **1**, no peak was observed at around *m*/*z* = 141, indicating that decomposition of **1** to methamidophos is improbable. ^{31}P-NMR signals at 27.13 ppm were assigned to the P–O–CH_3 and P–S–CH_3 groups of acephate. Upward shift at 2.88 and −5.88 ppm was observed in **1** as compared to acephate due to two different arrangements of –S–CH_3 and –O–CH_3

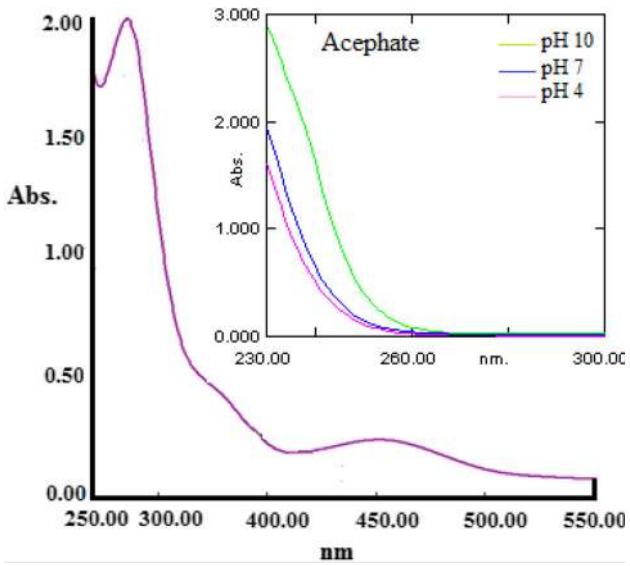

Fig. 1 UV–Vis spectra of **1** and of acephate

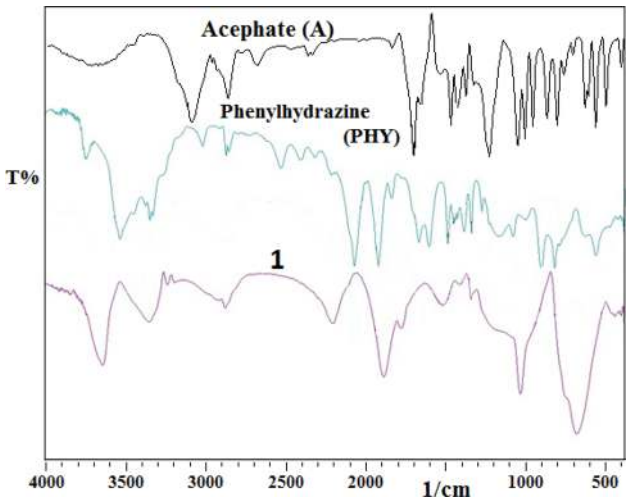

Fig. 2 FTIR spectrum of acephate, phenylhydrazine and **1**

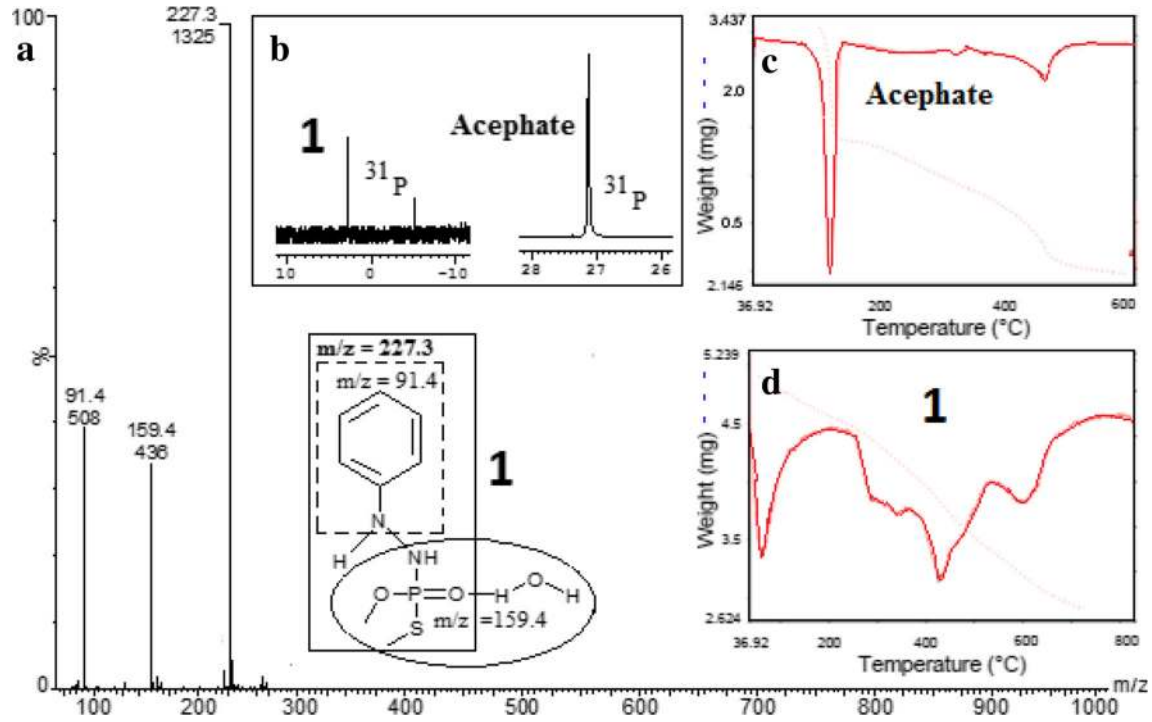

Fig. 3 Mass (ESI–MS), ^{31}P-NMR and thermal study (TGA) of acephate and **1**. **a** Mass analysis of **1**, **b** ^{31}P NMR spectra of **1** and of acephate, **c** thermal study of acephate and **d** thermal study of **1**

Table 1 Kinetic parameters of the acephate and **1** (for detail, see Supplementary Information S4)

Moiety	Main step	Thermodynamic parameters by TG/DTG analysis						
		T_p (K)	A (min^{-1})	Ea (kJ/mol)	ΔH (kJ/mol)	ΔS (kJ/mol)	ΔG (kJ/mol)	r^2
Acephate **1**	1st	450	9.1×10^{19}	9.54	5.79	0.167	−69.36	0.98
	2nd	698	6.3×10^{7}	62.15	−67.95	−0.068	−20.04	0.96

around phosphate atoms (Kumar et al. 2013a; Silberstein et al. 2005). It means both the signal showed downshift (10 and 12 times) with decrease in intensity (2 and 3 times) as compared to acephate (Fig. 3b).

The presence of water molecules in **1** was confirmed by the thermal study. Higher activation energy for thermal decomposition of **1** was observed (62.15 kJ/mol) as compared to acephate (9.54 kJ/mol) (Fig. 3c, d; Table 1). Thermal analysis (TGA) showed formation of stable new adduct as compared to parent acephate. In thermal analysis, it was observed that product **1** decomposed at higher temperature (698 K) (Table 1) as compared to acephate (450 K).

Mechanism

The final structure of **1** was confirmed by FTIR, ^{31}P-NMR, mass and thermal analysis data as sated above. Nucleophilic substitution reaction by attack of nucleophile phenylhydrazine (:NH_2–NH–) to acephate is responsible for the formation of product **1**. Both phosphate phosphorus and carbonyl carbon are electron deficient but because of more electropositive character of phosphorus, nucleophile attack on it leads to displacement of acetamide (Chen et al. 2014; Rosamilia et al. 2008) (Scheme 1).

Biology

Plant growth-promoting activities

Effect of **1** on plant growth-promoting strains was performed to check its toxic/negative effect compared to acephate at their different concentration levels, i.e., 25, 50, 100 and 200 µg/L. Effect on inhibition of siderophores production by acephate and **1** was determined on King's B (KB) medium using the literature reported method (Yasmin et al. 2009). Huge inhibition difference was obtained between acephate (more toxic) and **1** (less toxic) (Ahemada

Scheme 1 Synthesis scheme of **1**

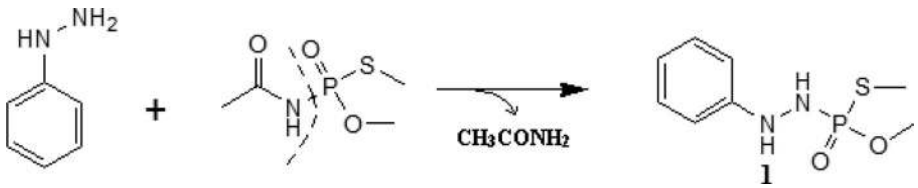

Table 2 Plant growth-promoting activities of acephate and **1**

Strain code	Conc. (ppm)	Acephate				Molecule **1**			
		SA (mean)[a]	IAA (mean)[a]	HCN	PS (mm)[b]	SA (mean)[a]	IAA (mean)[a]	HCN	PS (mm)[b]
1	0	0.81 ± 0.006*	0.74 ± 0.007*	+++	12 ± 2*	0.81 ± 0.006*	0.74 ± 0.004*	+++	12 ± 2*
	25	0.56 ± 0.004*	0.54 ± 0.006*	+	08 ± 0*	0.75 ± 0.004*	0.64 ± 0.006*	++	10 ± 2*
	200	0.14 ± 0.004*	0.42 ± 0.006*	−	05 ± 1*	0.45 ± 0.003*	0.53 ± 0.007*	+	09 ± 1*
2	0	0.75 ± 0.005*	0.72 ± 0.005*	++	11 ± 2*	0.75 ± 0.002*	0.72 ± 0.005*	++	11 ± 3*
	25	0.58 ± 0.007*	0.53 ± 0.004*	+	07 ± 1*	0.67 ± 0.004*	0.58 ± 0.005*	++	09 ± 2*
	200	0.21 ± 0.007*	0.44 ± 0.006*	−	05 ± 1*	0.49 ± 0.006*	0.49 ± 0.003*	+	08 ± 2*
3	0	0.89 ± 0.006*	0.69 ± 0.007*	+++	14 ± 0*	0.89 ± 0.005*	0.69 ± 0.006*	+++	14 ± 2*
	25	0.61 ± 0.006*	0.59 ± 0.008*	+	09 ± 2*	0.69 ± 0.005*	0.62 ± 0.005*	++	11 ± 1*
	200	0.24 ± 0.008*	0.39 ± 0.008*	+	06 ± 0*	0.44 ± 0.007*	0.58 ± 0.005*	+	09 ± 2*
4	0	0.84 ± 0.006*	0.71 ± 0.007*	++	15 ± 3*	0.84 ± 0.003*	0.71 ± 0.008*	++	15 ± 4*
	25	0.68 ± 0.005*	0.64 ± 0.006*	+	11 ± 2*	0.76 ± 0.006*	0.67 ± 0.006*	++	12 ± 2*
	200	0.19 ± 0.006*	0.51 ± 0.005*	−	08 ± 2*	0.59 ± 0.004*	0.61 ± 0.007*	+	09 ± 1*
5	0	0.86 ± 0.005*	0.73 ± 0.006*	+++	12 ± 3*	0.86 ± 0.007*	0.73 ± 0.004*	+++	12 ± 3*
	25	0.63 ± 0.004*	0.59 ± 0.005*	+	09 ± 1*	0.69 ± 0.005*	0.65 ± 0.005*	++	10 ± 1*
	200	0.21 ± 0.008*	0.51 ± 0.005*	−	06 ± 0*	0.51 ± 0.006*	0.56 ± 0.006*	+	08 ± 0*

1, *Rhizobium leguminosarum*; 2, *Arthrobacter citreus*; 3, *Pseudomonas fluorescens*; 4, *Bacillus brevis*; 5, *Salmonella typhimurium*; SA, siderophoric activities; IAA, indole acetic acid activities; HCN hydrogen cyanide production; PS, phosphate solubilization; +++, stand for deep brown color; ++, stand for light brown; −, stand for no color

* Statistically significant ($p \leq 0.05$) versus control

[a] Mean measured by comparing absorbance

[b] Mean measured by scale due to hole formation

and Kibret 2014). The siderophore production was reduced significantly ($p \leq 0.05$) in acephate compared to **1** (and is shown by notation acephate: **1**). At 25 µg/L, inhibition of plant growth-promoting strain compared to control was found by 30:17 % and 80:55 % over control was obtained at 200 µg/L (Table 2). Exact siderophore production by different bacteria in the presence of **1** was found in order: *B. brevis* > *R. leguminosarum* > *S. typhimurium* > *A. citreus* = *P. fluorescens* (supplementary Figure S2).

Phosphate solubilization was increased with the use of **1** as compared with acephate (Table 2). Among all strains at significant level ($p \leq 0.05$), *B. brevis* produced less phosphate solubilization (hole in mm) in the presence of **1.** Exact order of phosphate solubilization was found to be *R. leguminosarum* > *P. fluorescens* > *A. citreus* > *S. typhimurium* > *B. brevis* (supplementary Figure S3).

Rhizobacteria produce HCN to protect the growing plants from pathogen attack by direct killing of parasites (Ahemada and Kibret 2014). In this study, three concentrations of each acephate and **1** did affect negatively HCN synthesis, but very low effect of **1** was analyzed. In case of acephate, only two strains (*A. citreus*, *B. brevis*) were found to produce HCN (supplementary Fig. S4), while in the presence of **1** all strains (*R. leguminosarum*, *P. fluorescens*, *A. citreus*, *B. brevis* and *S. typhimurium*) produced HCN (Table 2).

In the medium, where acephate and **1** was not supplied, all strains produced indole acetic acid (IAA) in significant amount ($p \leq 0.05$). But, on comparison with acephate, **1** was producing higher concentration of IAA (Table 2). Among all strains at significant level ($p \leq 0.05$), *S. typhimurium* produced lowest amount of IAA in the presence of **1** compared to other strains and order of IAA production was: *A. citreus* > *B. brevis* > *R. leguminosarum* > *P. fluorescens* > *S. typhimurium*. It is worthy to mention that acephate shows inhibitory effect on plant growth-

promoting strains even at small concentrations. It could disrupt the bacterial community due to differences in sensitivity between microorganisms. Any modification of the environment which leads to a response by living organisms may be considered as a stress (Kumar et al. 2015a; Missous et al. 2007). The biotic stress observed in biology, is considered a global phenomenon, and can be extended to anthropogenic pressure such as genetic engineering or xenobiotic (including pesticides) pollution (Kumar et al. 2014; Thammavongs et al. 2008). The synthesized molecule **1** did not show significant effect on the growth of the tested bacteria w.r.t. their plant growth-promoting activities. More detail of plant growth activities by **1** can be seen in Supplementary Information S5.

*UV–Vis spectra and stability of **1**-BSA complexes*

An increase in the concentrations of **1** in the presence of BSA resulted increase in UV light absorption and shifting of BSA band at 279–274 nm that can be related to complex formation (Fig. 4). Molecule showed binding with BSA with a binding constants of 1.12 (±0.09) × 10^4 M^{-1}. The binding constant for **1**-BSA complex suggests a low affinity (<10^6) for complex formation, compared to strong ligand–protein complexes, with binding constants ranging from 10^6 to 10^8 M^{-1} (Bourassa et al. 2011; Kragh-Hansen 1990; Liu et al. 2004). In in vitro studies, organophosphate pesticides were not only found to bind with serine hydrolases but also to proteins that was not having serine as active site, e.g., Tyr 411 of human albumin and Lys 296 of mouse transferrin (Lockridge 2013). Higher the protein binding constant of agrochemicals or pesticides, higher will be the toxicity (Lockridge 2013; Kumar et al. 2013a). Interestingly, the low binding constant of **1** shows less toxicity of synthesized molecule toward protein interactions of organisms which is a major problem of maximum agrochemical especially in aquatic environment.

FTIR spectra of BSA and product-BSA complexes

Shifting of protein amide I band (mainly C=O stretch) and amide II band (C=N stretching coupled with N–H bending modes) which originally absorbs at 1653 and 1541 cm^{-1}, respectively (Byler and Susi 1986; Krimm and Bandekar 1986) was observed as **1** interacted with BSA protein (Fig. 5). In recent studies, the observed FTIR peaks for the free protein are reported to be: α-helix (1656 cm^{-1}), β-sheet (1618 and 1628 cm^{-1}), turn structure (1670 cm^{-1}), β-antiparallel (1693 and 1680 cm^{-1}) and random coil (1638 cm^{-1}) (Ahmed-Ouameur et al. 2006; Bourassa et al. 2010). The β-sheet structure is composed of two components at 1618 (inter β-strand) and 1628 cm^{-1} (intra β-strand) (hydrated) that are consistent with the spectroscopic current studies of bovine serum albumin (Ahmed-Ouameur et al. 2006; Bourassa et al. 2010; Byler and Susi 1986; Krimm and Bandekar 1986).

On addition of **1** (0.00125 mM) to BSA, decrease in intensity as well as shift (4 cm^{-1}) of the amide I band at 1658 cm^{-1} (BSA) was observed at 1654 cm^{-1}. In the spectrum of **1**-BSA complex, the reduction in intensity due to loss of protein structure of the amide I band was obtained and suggests major reduction in protein α-helical structure (Fig. 5) (Ahmed-Ouameur et al. 2006; Bourassa et al. 2010). The decrease in α-helix structure and increase in β-sheet and turn structures is indicative of protein destabilization upon interaction with **1**.

On quantitative analysis of BSA and **1**, free protein was found to have 69 % a-helix (1658 cm^{-1}), 12 % β-sheet (1620 cm^{-1}), 14 % turn structure (1676 cm^{-1}), 3 % β-antiparallel (1690 cm^{-1}) and 2 % random coil (1637 cm^{-1}) structure (Fig. 5). The results are consistent with the spectroscopic studies of bovine serum albumin previously reported (Ahmed-Ouameur et al. 2006; Bourassa et al. 2010). Upon interaction of **1**, a major decrease in α-helix from 69 % (free BSA) to 7.4 % (**1**-BSA at

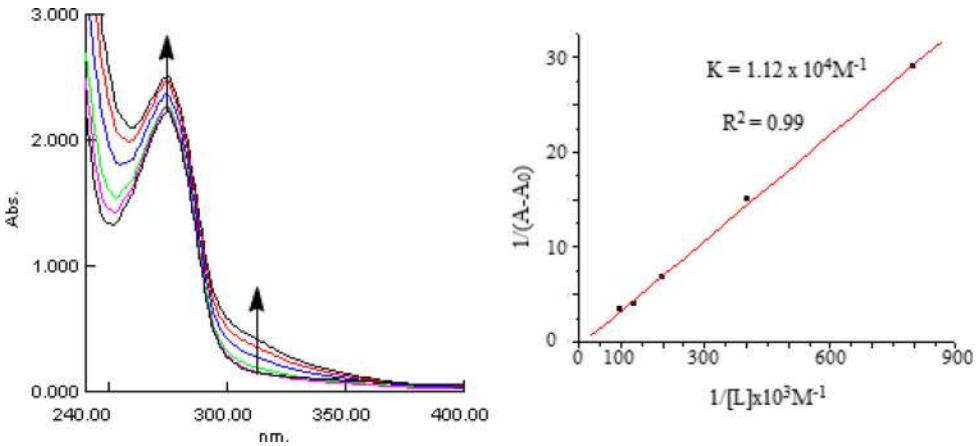

Fig. 4 UV–Vis study of **1**-BSA binding constant

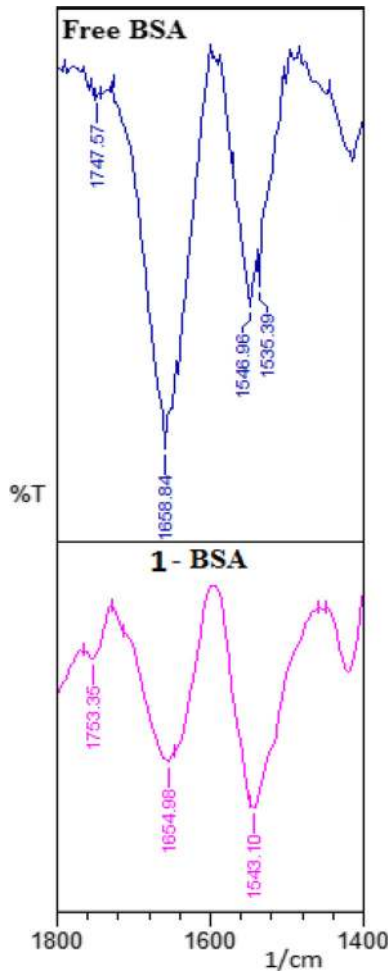

Fig. 5 FTIR spectrum of free BSA and **1**-BSA

0.00125 mM) was observed and 14 % in β-sheet (**1**-BSA, 0.00125 mM), 3.7 % in β-antiparallel (**1**-BSA, 0.00125 mM) and 4.7 % in random coil (**1**-BSA, 0.00125 mM) were obtained.

Computational study

Huckel charge densities and dipole–dipole interactions

Often in organic chemistry, the "partial" charge on an atom of a compound highlights the nucleophilic or electrophilic site. In the current study, Huckel charge densities were analyzed theoretically as tabulated in Table 3. From this analysis, one thing is clear that P atom was obtained to have maximum positive charge (1.857) and was found to have better site for nucleophilic attack and double-bonded oxygen attached to P is itself may act like a nucleophile with a negative charge 1.184. Huckel charge densities are useful quantities to illustrate the charge distributions which can give the information about how the molecules interact with another molecule in environmental compartments.

The optimized value of dipole–dipole interactions for the molecule **1** is 0.12, which is low, and it conforms that molecule **1** could interact or bind less with other living or organic molecules such as proteins, enzymes, DNA; consequently, molecule **1** may cause low harm to living organisms and total environment. Biggest impact of these interactions on living organisms was seen in past with protein folding (Campbell and Reece 2005; Le-Fèvre 1953). Every process of protein binding depends on net dipole–dipole interactions (Campbell and Reece 2005; Le-Fèvre 1953). From the analysis of these parameters of molecule **1**, it is clear that this molecule may interact with the proteins, enzymes, DNA and essential organic molecules with low binding constant as was proved by low value of **1**-BSA interactions.

Geometric parameters and vibrational frequencies

Bond length and bond angles of **1** have been optimized (Table 3). These parameters may help the future studies like single-crystal analysis of **1**. The optimized theoretical vibrational frequencies of product were found to be in good agreement with the corresponding experimental data (Table 4). The slight differences observed between the calculated and experimental values were observed mostly due to fact that the theoretical calculations were performed for the product in the gaseous phase, while the experimental results were obtained for the solid phase of the pesticides (Young 2001).

*Computational evaluation of structural analogs of **1** for physical and molecular properties*

Twelve new analogs of **1** were prepared computationally (Fig. 6) and compared with **1**. The HOMO–LUMO energy difference of analogs A1–A12 was calculated (Fig. 6; Table 5). It was obtained that all the molecules are non reactive due to their high energy difference. As per literature, the molecules with reduced HOMO–LUMO gaps <1.30 eV are chemically very reactive due to HOMO contribution to the decrease in the topological resonance energy (Aihara 1999). The observed value of energy difference for molecules A1–A12 lies between 33.311 and 1.542 eV. Hence, on the basis of HOMO–LUMO energy gap, the order of stability was: A11 $\gg$ A $\gg$ A9 = A6 > A10 > A8 > **1** = A2 = A3 > A1 > A4 > A12 > A5 $\gg$ > A7. But an interesting point was analyzed, i.e., once the phenyl molecule attached to **1,** it converted into least stable molecule A7 with energy gap 1.542 eV. Disturbance of planarity and polarity may a reason behind it, because N–N site potentially making the **1** more planar. The P atom of **1** is exactly the site that can be polarized, especially because N–N group, O–X group and S–Y groups attached to P are unequal.

Table 3 Optimized Huckel charges and geometric parameter for **1**

Huckel charges	Bond length (Å)	Bond angle (°)	Bond angle (°)
Geometric parameters of product including Huckel charges			
C −0.176 [C(1)]	C(1)–C(2) 1.387	H(27)–C(14)–H(26) 109.490	Lp(28)–N(8)–N(7) 109.500
C −0.024 [C(2)]	C(6)–C(1) 1.387	H(27)–C(14)–H(25) 110.562	H(21)–N(8)–P(9) 114.031
C −0.159 [C(3)]	C(1)–H(15) 1.067	H(27)–C(14)–O(12) 109.979	H(21)–N(8)–N(7) 114.741
C −0.032 [C(4)]	C(2)–C(3) 1.380	H(26)–C(14)–H(25) 110.378	P(9)–N(8)–N(7) 115.639
C −0.144 [C(5)]	C(2)–H(16) 1.074	H(26)–C(14)–O(12) 110.125	H(20)–N(7)–N(8) 111.651
C 0.135 [C(6)]	C(3)–C(4) 1.387	H(25)–C(14)–O(12) 106.264	H(20)–N(7)–C(6) 115.282
N 0.139 [N(7)]	C(3)–H(17) 1.070	H(24)–C(13)–H(23) 112.011	N(8)–N(7)–C(6) 115.324
N −0.275 [N(8)]	C(4)–C(5) 1.378	H(24)–C(13)–H(22) 110.472	C(4)–C(5)–H(19) 119.430
P 1.857 [P(9)]	C(4)–H(18) 1.072	H(24)–C(13)–S(11) 108.533	C(4)–C(5)–C(6) 120.640
O −1.184 [O(10)]	C(5)–C(6) 1.393	H(23)–C(13)–H(22) 110.981	H(19)–C(5)–C(6) 119.929
S −0.132 [S(11)]	C(5)–H(19) 1.070	H(23)–C(13)–S(11) 108.500	C(1)–C(6)–N(7) 122.839
O −0.484 [O(12)]	C(14)–H(27) 1.083	H(22)–C(13)–S(11) 106.117	C(1)–C(6)–C(5) 118.510
C −0.164 [C(13)]	C(14)–H(26) 1.079	Lp(30)–O(12)–Lp(29) 90.850	N(7)–C(6)–C(5) 118.627
C 0.064 [C(14)]	C(14)–H(25) 1.078	Lp(30)–O(12)–C(14) 109.500	C(3)–C(4)–H(18) 120.556
H 0.032 [H(15)]	C(13)–H(24) 1.078	Lp(30)–O(12)–P(9) 109.500	C(3)–C(4)–C(5) 120.774
H 0.028 [H(16)]	C(13)–H(23) 1.077	Lp(29)–O(12)–C(14) 109.500	H(18)–C(4)–C(5) 118.669
H 0.029 [H(17)]	C(13)–H(22) 1.077	Lp(29)–O(12)–P(9) 109.500	C(2)–C(3)–H(17) 120.633
H 0.029 [H(18)]	O(12)–C(14) 1.450	C(14)–O(12)–P(9) 123.201	C(2)–C(3)–C(4) 118.739
H 0.028 [H(19)]	S(11)–C(13) 1.890	C(13)–S(11)–P(9) 102.800	H(17)–C(3)–C(4) 120.626
H 0.092 [H(20)]	P(9)–O(12) 1.637	O(12)–P(9)–S(11) 106.677	C(1)–C(2)–H(16) 118.773
H 0.102 [H(21)]	P(9)–S(11) 2.225	O(12)–P(9)–O(10) 115.060	C(1)–C(2)–C(3) 120.830
H 0.048 [H(22)]	P(9)–O(10) 1.536	O(12)–P(9)–N(8) 96.629	H(16)–C(2)–C(3) 120.391
H 0.042 [H(23)]	N(8)–H(21) 1.010	S(11)–P(9)–O(10) 112.080	C(2)–C(1)–H(15) 118.950
H 0.047 [H(24)]	P(9)–N(8) 1.711	S(11)–P(9)–N(8) 108.756	C(2)–C(1)–C(6) 120.494
H 0.036 [H(25)]	N(7)–H(20) 1.007	O(10)–P(9)–N(8) 116.293	H(15)–C(1)–C(6) 120.554
H 0.034 [H(26)]	N(7)–N(8) 1.430	Lp(28)–N(8)–H(21) 90.360	
H 0.033 [H(27)]	C(6)–N(7) 1.418	Lp(28)–N(8)–P(9) 109.500	

Table 4 Optimized and experimental FTIR frequencies for **1**

Optimized frequencies (cm^{-1})[a]	Experimental frequencies[a]	Mode assignments	Shift values (cm^{-1})
3650	3640	*v*(O–H)	10
3350	3360	*v*(N–H)	10
1790	1890	*v*(N=N)	100
1671	1500	*v*(C=C)	121
980	1050	*v*(C–N), *v*(C–O), *v*(P=O)	70
835	830	*v*(P–O)	05
707	700	*v*(N–H) oop, monosub.	07

[a] Optimized frequencies are for gas phase, while experimental frequencies are in solid phase

Polarizabilities and the prediction of the biodegradation The computed averaged static dipole polarizability and dipole moment of molecules A1–A12 including **1** and acephate (A) were calculated. The component of the polarizability tensor was optimized along *z*-axis, i.e., along molecular axis. The values of average polarizabilities depend upon the positions of substituents bound to the moiety (Long 1982). The average polarizability ($\langle\alpha\rangle$) was calculated as per formula reported in the literature (Ostojic et al. 2014), i.e., $\langle\alpha\rangle = (\alpha_{xx} + \alpha_{yy} + \alpha_{zz})/3$. The values of dipole moment and average polarizability for all molecules are tabulated in Table 5. As per recent computational studies, the biodegradation is directly proportional to the average polarizability of molecule (Long 1982; Ostojic et al. 2014). On the basis of average polarizability, the order of biodecomposition is: A9 > A3 > A2 > A6 > **1** > A5 > A1 > A8 > A7 > A4 > A4 > A12 > A11 > A10.

A statistical relationship between polarizability of all the analogs was analyzed using origin 6.1 software. On the basis of substituents, analogs were divided into four series 1–4. Variations in polarizability of analogs were compared in all series w.r.t. acephate. Overall value of R^2 was 0.54, indicating that all the analogs having significant ($p < 0.05$)

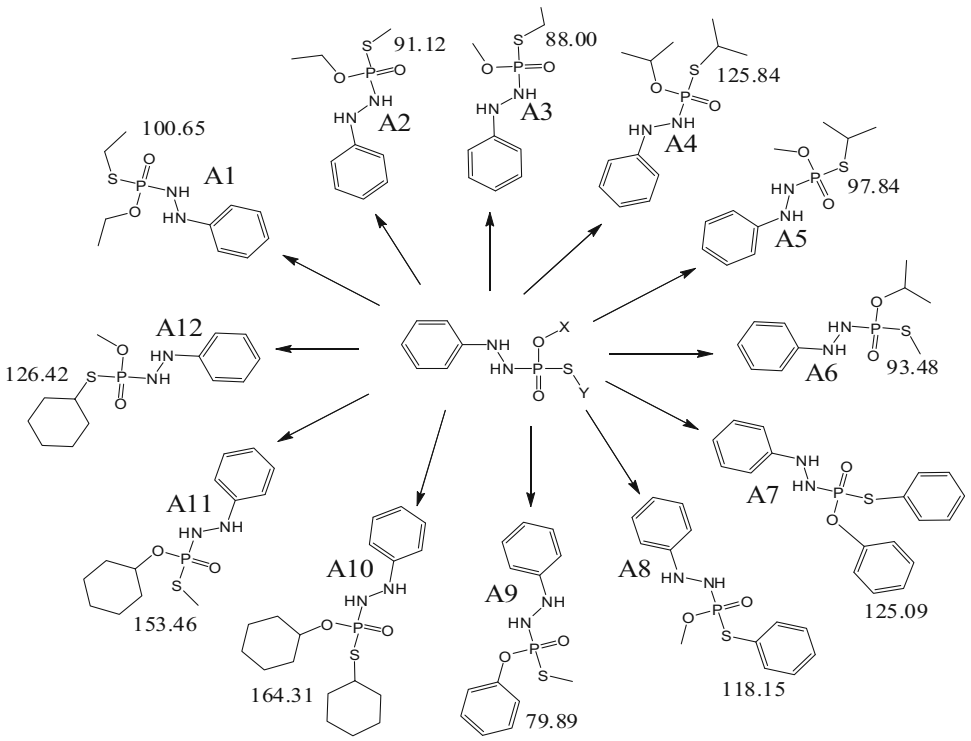

Fig. 6 Chemical structures of new derivatives of **1** and values of average polarizability ⟨α⟩ in eV

Table 5 Statistical parameters of electronic and physicochemical properties of analogs of **1**

Code	Analog		Statistics		Physicochemical			Electronic		
	X	*Y*	Series	R^2	E_{Steric} (kcal/mol)	⟨α⟩	Dipole (D)	E_{LUMO} (eV)	E_{HOMO} (eV)	Δ*E* (eV)
1	CH_3	CH_3			23.36	94.68	2.88	0.490	−6.319	6.809
A1	C_2H_5	C_2H_5	1[a]	0.98	25.38	100.65	4.55	0.490	−6.316	6.806
A2	C_2H_5	CH_3			23.10	91.12	4.99	0.490	−6.319	6.809
A3	CH_3	C_2H_5			23.98	88.00	5.79	0.490	−6.319	6.809
A4	C_3H_9	C_3H_9	2[a]	0.95	29.90	125.84	6.16	0.490	−6.310	6.800
A5	CH_3	C_3H_9			24.56	97.84	6.63	0.490	−6.307	6.797
A6	C_3H_9	CH_3			29.04	93.48	5.99	0.490	−6.353	6.843
A7	C_6H_6	C_6H_6	3[a]	0.93	21.62	125.09	6.13	0.490	−1.052	1.542
A8	CH_3	C_6H_6			20.59	118.15	5.20	0.490	−6.321	6.811
A9	C_6H_6	CH_3			23.57	79.89	5.04	0.490	−6.353	6.843
A10	C_6H_{12}	C_6H_{12}	4[a]	0.96	38.84	164.31	6.01	0.490	−6.351	6.841
A11	C_6H_{12}	CH_3			32.87	153.46	2.27	26.97	−6.341	33.311
A12	CH_3	C_6H_{12}			29.29	126.42	5.71	0.490	−6.309	6.799
A	–	–			20.19	55.57	4.30	2.313	−10.01	12.323

[a] Series 1,2,3 and 4 include acephate (A)

difference in polarizability. The R^2 value for series 1 (A, A1–A3) was 0.98, for series 2 (A, A4–A6) was 0.95, for series 3 (A, A7–A9) was 0.93 and for series 4 (A, A10–A12) was 0.96 (Fig. 7). Among the four series, order of biodecomposition was found in order 1 > 3 > 2 > 4.

Conclusion

Phenylhydrazine binds with acephate through nucleophilic attack on it. The obtained product neutralized toxic effect of acephate on plant growth-promoting strains. The binding

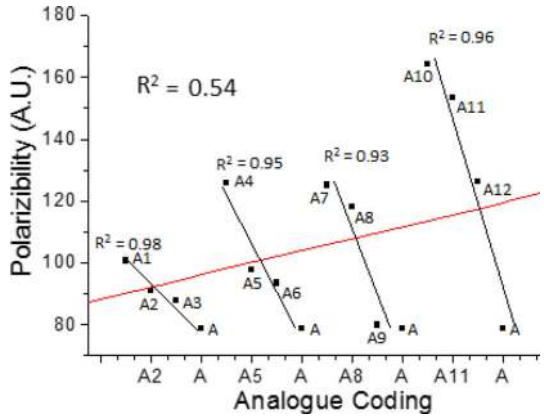

Fig. 7 Relationship with different derivatives of **1**

of **1** to BSA protein and interactions with PGPR strains may not be expected to explain the toxicity directly, but it can serve as a model to study the effect of **1** and other pesticides on proteins and microorganisms. A combined experimental and computational study was developed with the aim of evaluating and understanding the structural, energetic and stability of **1**.

Safety

Acephate is an organophosphate pesticide that inhibits the activity of cholinesterase. Direct contact with this should be avoided. Work performed with this pesticide in the open should take place in a fume hood using gloves and eye protection.

Acknowledgments Author would like to acknowledge University Grant Commission—India (for RGNF; National Fellowship for Vijay Kumar), Lovely Professional University, SAIF, Cochin, and SAIF, Punjab University, Chandigarh, for instrument facilities.

Compliance with ethical standards

Conflict of interest We have no conflict of interest.

References

Abdi K, Nafisi SH, Manouchehri F, Bonsaii M, Khalaj A (2012) Interaction of 5-Fluorouracil and its derivatives with bovine serum albumin. J Photochem Photobiol B 107:20–26

Ahemada M, Kibret M (2014) Mechanisms and applications of plant growth promoting rhizobacteria: current perspective. J King Saud Univ Sci 26:1–20

Ahmed-Ouameur A, Diamantoglou S, Sedaghat-Herati MR, Nafisi S, Carpentier R, Tajmir-Riahi HA (2006) The effects of drug complexation on the stability and conformation of human serum albumin: protein unfolding. Cell Biochem Biophys 45:203–214

Aihara J (1999) Reduced HOMO–LUMO gap as an index of kinetic stability for polycyclic aromatic hydrocarbons. J Phys Chem A 103:7487–7495

Bourassa P, Kanakis CD, Tarantilis P, Pollissiou MG, Tajmir-Riahi HA (2010) Resveratrol, genistein, and curcumin bind bovine serum albumin (dagger). J Phys Chem B 114:3348–3354

Bourassa P, Dubeau S, Maharvi GM, Fauq AH, Thomas TJ, Tajmir-Riahi HA (2011) Locating the binding sites of anticancer tamoxifen and its metabolites 4-hydroxytamoxifen and endoxifen on bovine serum albumin. Eur J Med Chem 46:4344–4353

Byler DM, Susi H (1986) Examination of the secondary structure of proteins by deconvolved FTIR spectra. Biopolymers 25:469–487

Campbell NA, Reece JB (2005) Biology. Pearson Benjamin Cummings, San Francisco

Chen SY, Zeng RS, Zou JP, Asekun OT (2014) Copper-catalyzed coupling reaction of arylhydrazines and trialkylphosphites. J Org Chem 79:1449–1453

Connors K (1987) Binding constants: the measurement of molecular complex stability. Wiley, New York

David T (1998) The greening of the green revolution. Nature 396:211–212

Kragh-Hansen U (1990) Structure and ligand binding properties of human serum albumin. Dan Med Bull 37:57–84

Krämer W (2007) Modern crop protection compounds, vol 1. Wiley, New Jersey

Krimm S, Bandekar J (1986) Vibrational spectroscopy and conformation of peptides, polypeptides, and proteins. Adv Protein Chem 38:181–364

Kumar V, Upadhyay N, Wasit AB, Simranjeet S, Parvinder K (2013a) Spectroscopic methods for the detection of organophosphate pesticides: a preview. Curr World Environ 8(2):313–318

Kumar V, Upadhyay N, Singh S, Singh J, Kaur P (2013b) Thin-layer chromatography: comparative estimation of soil's atrazine. Curr World Environ 8:469–473

Kumar V, Upadhyay N, Kumar V, Kaur S, Singh J, Singh S, Datta S (2014) Environmental exposure and health risks of the insecticide monocrotophos: a review. J Biodivers Environ Sci 5:111–120

Kumar V, Upadhyay N, Kumar V, Sharma S (2015a) A review on sample preparation and chromatographic determination of acephate and methamidophos in different samples. Arab J Chem. doi:10.1016/j.arabjc.2014.12.007

Kumar V, Singh S, Singh J, Upadhyay N (2015b) Potential of plant growth promoting traits by bacteria isolated from heavy metal contaminated soils. Bull Environ Contam Toxicol 94:807–814

Kumar V, Upadhyay N, Kumar V, Sharma S (2015c) Interactions of atrazine with transition metal ions in aqueous media: experimental and computational approach. 3 Biotech. doi:10.1007/s13205-015-0281-x

Kumar V, Upadhyay N, Manhas N (2015d) Designing, syntheses, characterization, computational study and biological activities of silver-phenothiazine metal complex. J Mol Struct 1099:135–141

Le-Fèvre RJW (1953) Dipole moments; their measurement and application in chemistry. Methuen, London

Liu J, Tian J, Hu Z (2004) Binding of isofraxidin to bovine serum albumin. Biopolymers 73:443–450

Lockridge O (2013) Noncholinesterase protein targets of organophosphorus pesticides. Adv Mol Toxicol 7:179–205

Long DA (1982) The polarizability and hiperpolarizability tensors. In: Kiefer W, Long DA (eds) Non-linear Raman spectroscopy and its chemical applications. Reidel, Dordrecht, pp 99–112

Missous G, Thammavongs B, Dieuleveux V, Gueguen M, Panoff JM (2007) Improvement of the cryopreservation of the fungal starter *Geotrichum candidum* by artificial nucleation and temperature downshift control. Cryobiology 55:66–71

Ostojic BD, Stankovic B, Đor-devic DS (2014) Theoretical study of the molecular properties of dimethylanthracenes as properties for the prediction of their biodegradation and mutagenicity. Chemosphere 111:144–150

Painter P, Harding MM, Beeby PJ (1998) Synthesis and interaction with human serum albumin of the first 3, 18-disubstituted derivative of bilirubin. J Chem Soc, Perkin Trans 1:3041–3044

Prasad R, Upadhyay N, Kumar V (2013) Simultaneous determination of seven carbamate pesticide residues in gram, wheat, lentil, soybean, fenugreek leaves and apple matrices. Microchem J 111:91–96

Rosamilia AE, Aricò F, Tundo P (2008) Reaction of the ambident electrophile dimethyl carbonate with the ambident nucleophile phenylhydrazine. J Org Chem 73:1559–1562

Silberstein RM, Webster FX, Kiemle DJ (2005) Spectroscopic identification of organic compounds, 7th edn. New Jersey, Willy

Thammavongs B, Denou E, Missous G, Guéguen M, Panoff JM (2008) Response to environmental stress as a global phenomenon in biology: the example of microorganisms. Microbes Environ 23:20–23

Wasim A, Dwaipayan S, Ashim C (2009) Impact of pesticides use in agriculture: their benefits and hazards. Interdiscip Toxicol 2:1–12

Yasmin F, Othman R, Sijam K, Saad MS (2009) Characterization of beneficial properties of plant growth-promoting rhizobacteria isolated from sweet potato rhizosphere. Afr J Microbiol Res 3(11):815–821

Young DC (2001) Computational chemistry a practical guide for applying techniques to real-world problems (electronics). Wiley, New York